2022

Mercury Methylation in Oxic Sub-Polar Marine Regions Linked with Nitrification

Marissa Collins Despins
Wright State University

MERCURY METHYLATION IN OXIC SUB-POLAR MARINE REGIONS LINKED WITH NITRIFICATION

A thesis submitted in partial fulfillment of the
requirements for the degree of
Master of Science

By

MARISSA COLLINS DESPINS
B.S., University of Wisconsin – La Crosse, 2019

2022
Wright State University

WRIGHT STATE UNIVERSITY
GRADUATE SCHOOL

June 30, 2022

I HEREBY RECOMMEND THAT THE THESIS PREPARED UNDER MY SUPERVISION BY Marissa Collins Despins ENTITLED Mercury Methylation in Oxic Sub-Polar Marine Regions Linked with Nitrification BE ACCEPTED IN PARTIAL FULFILLMENT OF THE REQUIREMENTS FOR THE DEGREE OF Master of Science.

Silvia E. Newell, Ph.D.
Thesis Director

Rebecca E. Teed, Ph.D.
Interim Chair, Department of Earth & Environmental Sciences

Committee on
Final Examination

Robert P. Mason, Ph.D.

Ana M. Aguilar-Islas, Ph.D.

Barry Milligan, Ph.D.
Vice Provost for Academic Affairs
Dean of the Graduate School

ABSTRACT

Despins, Marissa Collins. M.S. Department of Earth and Environmental Science, Wright State University, 2022. Mercury Methylation in Oxic Sub-Polar Regions Linked with Nitrification.

Methylmercury (MeHg) is a neurotoxin that bioaccumulates to potentially harmful concentrations in Arctic marine wildlife and in those that consume them. Monitoring and modeling MeHg bioaccumulation and biogeochemical cycling in the ocean requires understanding of the mechanisms behind net mercury (Hg) methylation. The key functional gene for Hg methylation, *hgcAB*, is widely distributed throughout ocean basins and spans multiple microbial phyla. While multiple microbially-mediated anaerobic pathways for Hg methylation are known, in the ocean, the majority of *hgcA* homologs have been found in oxic subsurface waters, in contrast to other ecosystems. In particular, microaerophilic *Nitrospina*, a genera of nitrite-oxidizing bacteria containing a *hgcA*-like sequence, has been proposed as a potentially important Hg methylator in upper ocean waters. The objective of this work was therefore to examine the potential of nitrifiers as Hg methylators and quantify total Hg and MeHg across three Arctic Seas (the Gulf of Alaska, the Bering Sea and the Chukchi Sea) in regions where *Nitrospina* are likely present. In Spring 2021, samples for Hg analysis were obtained from all sites with a trace metal clean rosette. Hg methylation rates were quantified in concert with nitrification rates using on-board incubation experiments with Hg and $^{15}NH_4^+$ stable isotope additions. A significant correlation between Hg methylation and nitrification was

observed across all sites, with the strongest correlation in the Chukchi Sea. *Nitrospina*-specific *hgcA*-like genes were detected at all sites. This study, linking Hg methylation and nitrification in oxic seawater, furthers understanding of MeHg cycling in these high latitude waters and the ocean in general. Furthermore, these studies inform predictions of how climate and human interactions could influence MeHg concentrations in the Arctic region in the future.

TABLE OF CONTENTS

TABLE OF CONTENTS (Continued)

Page

LIST OF FIGURES

Page

LIST OF TABLES

Page

AKNOWLEDGEMENTS

I would like to thank my advisor, Silvia Newell, for adopting me into your lab. Over the past two years, I've grown and become more confident as a scientist under your mentorship. Thank you for introducing and guiding me through the molecular world. Ana, thank you for introducing me to trace metal oceanographic sampling and cruise life. I'm very thankful to have had opportunity to operate your CTD. Thank you Rob, for taking me in as an honorary member of Team Hg and sharing your enthusiasm and excitement for Hg science. I appreciate you all for going above and beyond this past year and look forward to working with you in the future.

I thank chief scientists Russell Hopcroft and Tyler Hennon, the NGA LTER, and the captain and crew of the *R/V Sikuliaq*. I also thank Lauren Barrett and Penny Vlahos for contributing nutrient data, Yipeng He and Hannah Inman for contributing ambient Hg data, Lindsay Starr and Justin Myers for help with analyses, Carl Lamborg for assisting in Hg rate experiments, Caitlin Gionfriddo for providing *Nitrospina hgcA* amplicons and the UC – Davis stable isotope laboratory. Chad Hammerschmidt, thank you for the favorable recommendation to go on the cruise and for allowing me to use your lab. Thank you to WestRock scholarship program and the WSU EES graduate teaching assistantship program for funding my time at WSU.

Lastly, I thank my family, friends, and past mentors for their continued support and encouragement.

This thesis would not be possible without these contributions and efforts.

I. INTRODUCTION

The harmful bioaccumulating neurotoxin, methylmercury (MeHg), has increased over the past 150 years in Arctic mammals, resulting in high concentrations in the Canadian Arctic and Gulf of Alaska (GOA) marine predators (Wang *et al.,* 2018; Beckmen *et al.,* 2002; Lehnherr *et al.,* 2011; Dietz *et al.,* 2009). Consumption of high trophic level marine organisms serves as the main MeHg exposure route to humans (Sunderland *et al.,* 2007). In the early 2000s, Canadian and Greenlandic Inuit women were found, on average, to have higher blood mercury levels than the informal mercury (Hg) human blood guideline, with some communities surpassing the increased risk range set by Health Canada (Dietz *et al.,* 2013). Elevated MeHg levels in the body can result in neurodevelopmental effects, decrease in motor, psychomotor, visual, and cognitive functions and increased risk of cardiovascular disease (Mergler *et al.,* 2007; Clarkson and Magos, 2006). These health effects are exacerbated in fetuses of child-bearing mothers with elevated MeHg blood levels (Clarkson and Magos, 2006). The health of indigenous communities that rely on marine predators, both fish and mammals, as a food source continues to be an area of concern as MeHg blood concentrations of Arctic women still remain high (AMAP Assessment 2021). Mercury concentrations in ocean surface waters have been increasing since industrialization, with concurrent increases in marine MeHg concentrations (Lamborg *et al.,* 2014). Monitoring and modeling these increases in MeHg and drivers of MeHg production in the ocean require an understanding of the mechanisms behind Hg methylation.

Mercury Cycling

The Hg pool includes three differing species: gaseous elemental (Hg^0), MeHg (monomethylmercury and dimethylmercury), and inorganic divalent (Hg^{II}) (Fitzgerald *et al.,* 2007). As of 2018, the global estimate of anthropogenic Hg emissions was 2500 $\pm$ 500 Mg $year^{-1}$ (Outridge *et al.,* 2018). While western countries have decreased their Hg burden, countries with fast economic growth have increased their Hg emissions (Pirrone *et al.,* 2010). Global Hg emission models predict a 96% increase in emissions relative to 2015 if no reduction action is taken (Pacyna *et al.,* 2016). These increases are predicted to have a negative impact on the Arctic, as east Asian countries are a large source of anthropogenic Hg production and deposition in the Arctic (Schartup *et al.,* 2022). If no action is taken, models predict a significant increase in global human health cost (Zhang *et al.,* 2021). With the implementation of the Minamata Convention on Mercury in 2017, a treaty that is driving policy limiting Hg emissions and waste production, global anthropogenic Hg emissions are predicted to decrease by 2050 (Minamata Convention of Mercury: Article 1; Zhang *et al.,* 2021). Despite this predicted decrease in emissions, legacy Hg persists in the environment (Horowitz *et al.,* 2014).

The largest source of Hg^{II} to the ocean is through atmospheric deposition (Mason *et al.,* 2012). The current Hg exchange flux between the atmosphere and Arctic Ocean is 64.5 $\pm$ 19.8 Mg Hg yr^{-1} (Dastoor *et al.,* 2022). This exchange is influenced by atmospheric Hg depletion events (AMDE), which is the net loss of atmospheric Hg^0 through oxidation and subsequent deposition. These AMDE occur in spring in the Arctic and result in Hg sinks to first year ice and snow (Ariya *et al.,* 2004; Schroeder *et al.,* 1998). Total annual accumulated Hg deposition with Arctic AMDE yields deposition

around Alaska ranging from 12-25 μg m^{-2} Hg yr^{-1} (Ariya *et al.,* 2004). This increase in Hg deposition on melting first year ice and snow could result in an increase in dissolved and particulate Hg in Arctic waters. Rivers also serve as an important source of Hg^{II} to Arctic coastal zones, when compared to other oceans (Zolkos *et al.,* 2020; Sørensen *et al.,* 2016). Glacial retreat, melting permafrost, atmospheric deposition, and snowpack melt within Arctic watersheds all serve as sources of Hg to Arctic rivers. Arctic watersheds have the potential to yield the highest riverine Hg export to the ocean (Dastoor *et al.,* 2022). The Yukon River receives 5-10 μg Hg m^{-2} yr^{-1} across its watershed (Dastoor *et al.,* 2022). On average the Yukon River outflow delivers 227,000 ft^3 s^{-1} of freshwater to the Bering Sea (Brabets *et al.,* 2000) and yields 17.9 ng Hg L^{-1} in spring (Zolkos *et al.,* 2020). This is the highest Hg export of all six major Arctic Rivers (Zolkos *et al.,* 2020). It is estimated that rivers cumulatively discharge 41 $\pm$ 4 Mg Hg yr^{-1} to the Arctic Ocean (Sonke *et al.,* 2018; Zolkos *et al.,* 2020, Dastoor *et al.,* 2022). In comparison, atmospheric inputs are estimated at 64.5 ± 19.8 Mg Hg yr^{-1} (Dastoor *et al.,* 2022). Once in the marine water column, inorganic Hg^{II} is scavenged by sinking and suspended particles, resulting in sequestration into the benthos (Lamborg *et al.,* 2016). On the shelf in the Arctic Ocean, particle scavenging accounts for a loss of 122 $\pm$ 55 Mg Hg yr^{-1} from the surface waters to the benthos (Dastoor *et al.,* 2022). Additionally, Hg^{II} is reduced to Hg^0 and lost to the atmosphere via gas exchange (Mason *et al.,* 1994; Sørensen *et al.,* 2016). A separate fraction of Hg^{II} is transformed into its organic counterpart, MeHg (Fitzgerald *et al.,* 2007; Mason and Fitzgerald, 1991).

Higher concentrations of MeHg have been measured on the continental shelf when compared to the open ocean in the western Arctic Ocean and western GOA

(Agather *et al.,* 2019). Throughout the summer, the Alaskan Coastal Current (ACC) brings a large volume of freshwater derived from terrestrial runoff (via the Copper River outflow) to the coastline, resulting in a large salinity gradient in the GOA (Stabeno *et al.,* 2016). Similarly, in the Bering Strait, a low salinity signal is seen from the Yukon River outflow, also resulting in a large salinity gradient. These riverine inputs are an important source of Hg (Zolkos *et al.,* 2020). Upwelling currents along the Aleutian Islands and the shelf slope in the Bering Sea aid in the re-suspension and transport of nutrients and organic matter (Swift and Aagaard, 1976; Kelley *et al.,* 1971). The variability in the concentration of suspended particulates, water depth, and distance from the shelf are hypothesized to influence Hg methylation by particle bound microorganisms during the re-mineralization of riverine and resuspended benthic organic matter (Hammerschmidt and Fitzgerald, 2006; Capo *et al.,* in review; Lehnherr *et al.,* 2011). High MeHg concentrations have been observed just below the productive surface layer in the Arctic Ocean, Bering Sea, Northwest Atlantic and the North Pacific (U.S. GEOTRACES Cruise: GN01) (Wang *et al.,* 2018; Heimbürger *et al.,* 2015; Agather *et al.,* 2019; Sunderland *et al.,* 2009; Jonsson *et al.,* 2022; Schartup *et al.,* 2015). This MeHg maximum is shallower than in equatorial regions (Bowman *et al.,* 2016; Kim *et al.,* 2017). Mercury concentrations have yet to be published east of Kodiak Island in the GOA, but it is predicted to show a similar MeHg vertical distribution as the North Pacific. These shallow MeHg maxima cause a higher rate of bioaccumulation as these are oxic regions with increased primary production (Heimbürger *et al.,* 2015; Wang *et al.,* 2018).

Mercury methylation occurs through biotic and abiotic processes (Fitzgerald *et al*., 2007). Although possible, abiotic Hg methylation is less favorable as optimum conditions, such as high methyl-cobalamin concentrations and acidic waters, are rare in the ocean (Celo *et al*., 2006). Microbially-mediated Hg methylation occurs in conjunction with other anaerobic biogeochemical processes such as iron and sulfate reduction, and methanogenesis (Benoit *et al*., 2003, Gilmour *et al*., 2013), although *in-situ* Hg methylation has been observed in the oxic water column (Lehnherr *et al*., 2011; Munson *et al*., 2018; Starr *et al*., in review). Previous studies attribute dissolved and particulate MeHg in the upper oxic marine water column to release from re-suspended and re-mineralized organic matter from anoxic sediments along coastal regions (Hammerschmidt and Fitzgerald, 2006), but there is also the potential for methylation through other processes. Anoxic microenvironments in marine snow are also hypothesized to play a role in surface ocean Hg methylation (Ortiz *et al*., 2015). With low benthic-pelagic coupling in the central ocean, and given the rate of photo-degradation and demethylation of MeHg in the surface waters (DiMento and Mason, 2017; Munson *et al*., 2018), the question remains: by what mechanism is biotic Hg methylation occurring in the oxic surface waters at high latitudes? Lehnherr *et al*., (2011) developed a simple model based on their methylation and demethylation studies that estimated biotic MeHg formation accounts for 47% ($\pm$ 62%) of MeHg present in polar marine waters but did not provide a mechanism for this process.

Microbial Interactions

The key functional gene for Hg methylation, *hgcAB*, is widely distributed throughout all ocean basins and spans multiple microbial phyla, including aerobic and

anaerobic microorganisms (Parks *et al*., 2013; Gilmour *et al*., 2013; Gionfriddo *et al*., 2020; Villar *et al*., 2020). Drivers and regulators of the Hgc pathway and Hg methylation in oxic waters are poorly understood, resulting in critical, fundamental knowledge gaps about Hg methylation in the ocean water column (Bowman *et al*., 2020). The Hgc operon contains two key functional gene subunits: *hgcA* and *hgcB* (Parks *et al*., 2013). The conserved regions of *hgcA* encodes the methyltransferase enzyme, a corrinoid binding domain, which transfers the methyl group to Hg^{II} (Parks *et al*., 2013; Cooper *et al*., 2020). The *hgcB* gene encodes the ferredoxin protein which facilitates the reduction of the corrinoid center in *hgcA* (Parks *et al*., 2013; Cooper *et al*., 2020). While all Hg methylating microbes contain *hgcA*, *hgcB* is hypothesized not to always be needed as the cobalamin binding protein in *hgcA* could potentially carry out the reduction step (Gionfriddo *et al*., 2016, Podar *et al*., 2015; Cooper *et al*., 2020). All currently confirmed pathways for MeHg production are anaerobic and require anoxic conditions including bacteria and archaea from *Firmicutes*, *Deltaproteobacteria* and *Methanomicrobia* clades (Gilmour *et al*., 2013). However, across all ocean basins, 78% of discovered *hgcA* homologs have been found in oxic subsurface waters (Villar *et al*., 2020). In recent years, a new aerobic pathway for microbial mediated Hg methylation has been suggested, but the functionality of these *hgcAB* genes in oxic conditions have not yet been confirmed in culture (Gionfriddo *et al*., 2020). The currently described aerobic putative Hg methylating microbes belong to two nitrite-oxidizing clades, *Nitrospina* and *Nitrospira* (Gionfriddo *et al*., 2021). Microaerophilic *Nitrospina* was discovered to contain *hgcA*-like sequences in brine samples recovered from Antarctic sea ice (Gionfriddo *et al*., 2016). *Nitrospina* contains the conserved region of *hgcA* necessary for Hg methylation,

but not an *hgcB*-like gene (Bowman *et al*., 2020; Cooper *et al*., 2020). In addition to anaerobic Hg methylating microbes, *Nitrospina hgcA*-like genes have been recovered from Arctic and North Pacific seawater metagenomes, suggesting *Nitrospina* may play a role in Hg methylation in polar regions (Bowman *et al*., 2020; Tada *et al*., 2021). *hgcAB* genes from *Nitrospira,* the other currently described putative aerobic Hg methylator, have only been recovered from freshwater sediment and tidal marsh metagenomes (Gionfriddo *et al*., 2020; Christensen *et al*., 2019). Unlike all other currently described Hg methylating microbes, *Nitrospina hgcA*-like sequences have been found across all ocean basins, including the Arctic Ocean (Villar *et al*., 2020; Bowman *et al*., 2020; Tada *et al*., 2021; Tada *et al*., 2020). As the most widely distributed microaerophilic putative Hg methylating microbe, it is hypothesized that *Nitrospina* may play a key role in global MeHg production in the ocean subsurface (Villar *et al*., 2020), although *in situ* measurements of Hg methylation rates by cultured *Nitrospina* have yet to be conducted.

Nitrification

Chemolithoautotrophic nitrite oxidizing bacteria (NOB), such as *Nitrospina*, utilize oxygen, derived from water molecules, as the terminal electron acceptor in carbon-based metabolism (Lüker *et al*., 2013). Nitrite (NO_2^-) oxidation, catalyzed by NOB, is the second step of nitrification (Delwiche, 1970). Nitrification is a two-step aerobic reaction occurring throughout the ocean water column (Ward, 2008). The first reaction, ammonia (NH_3) oxidation, is facilitated by NH_3 oxidizing bacteria and archaea. This is the rate-limiting step of nitrification and thus drives nitrate (NO_3^-) production in the ocean (Ward, 2008). Nitrification primarily occurs in the euphotic zone, peaking near the NO_2^- maximum in the water column (Lomas and Lipschultz, 2006; Newell *et al*., 2013), but

has been measured in the ocean sub-surface (Shiozaki *et al*., 2016). Yool *et al*., (2007) estimated the global marine specific nitrification rate constant to be 0.162 d^{-1}. It is predicted that around half of the NO_3^- produced through nitrification is assimilated into phytoplankton biomass (Yool *et al*., 2007). While a high-nutrient region, the sub-Arctic has been shown to have lower NO_3^- assimilation than equatorial coastal regions due to iron (Fe) limitation, causing a low-chlorophyll zone (Boyd *et al*., 2004; Shiozaki *et al*., 2016; Aguilar-Islas *et al*., 2007). Nitrification rates in the high latitude waters are lower than equatorial regions and are mainly controlled by light transmittance, micro- and macro nutrient availability, such as ammonium (NH_4^+), copper (Cu), and Fe, microbial community composition, and dissolved oxygen (DO) concentrations (Boyd *et al*., 2004; Ward 2008; Shiozaki *et al*., 2016).

Mercury Methylation and Nitrification

Recently, nitrification rates in the oxic subsurface of the equatorial Atlantic were quantified in tandem with Hg methylation rates. A significant positive correlation was reported between nitrification and Hg methylation rate potentials in the Amazon River Plume (Starr *et al*., in review). In these samples, *Nitrospina*-specific *16S* transcripts were correlated with both nitrification and Hg methylation rate potentials, but *Nitrospina*-specific *hgcA*-like gene abundance was not investigated (Starr *et al*., in review). This correlation and evidence of *Nitrospina* suggests that the same microbes could be responsible for both Hg methylation and nitrification in other oxic marine waters, particularly where *Nitrospina* has been previously found, such as the Arctic (Bowman *et al*., 2020). Mercury methylation rates have yet to be quantified in concert with both *Nitrospina*-specific *hgcA*-like gene presence and nitrification. The objective of this study

was therefore to investigate this newly discovered putative microbially-mediated Hg methylation pathway previously shown to coincide with nitrite oxidation. We hypothesized that: (1) There will be a positive correlation between Hg methylation rates and nitrification rates in the Bering and Chukchi Seas and GOA; (2) *Nitrospina*-specific *hgcA*-like genes will be found in the Bering and Chukchi Seas and GOA; and (3) Ambient Hg and nutrient concentrations will not be correlated with rate potentials as other biogeochemical processes are occurring.

II. METHODS

Sample Collection

Seawater samples were collected between April and June 2021 aboard the *R/V Sikuliaq* in the GOA, Bering Sea, and Chukchi Sea. Samples were collected during three oceanographic cruises: Northern Gulf of Alaska Long Term Ecological Research (NGA LTER), Bering and Aleutian Internal Tide Mixing (BAITMIX) and Hg Cycling in the Arctic (Table S1). Water samples were collected at a single depth, the chlorophyll *a* maximum, at 18 individual stations (Figure 1; Table S1). The chlorophyll *a* maximum was selected as previous studies have shown *in situ* Hg methylation at the chlorophyll *a* maximum (Munson *et al.,* 2018; Starr *et al.,* in review). Five stations span the GOA with varying distances from the Copper River outflow and the shoreline. The other 13 stations are along a transect extending north through the Bering and Chukchi Seas. The ship-owned SeaBird 911+ CTD rosette was used to assess the chlorophyll *a* maximum during the down cast, which determined the sampling depth. During the downcast, other water quality parameters were measured such as chlorophyll *a*, salinity, DO, photosynthetically active radiation (PAR), NO_2^-, temperature, and pressure. Due to limited water allowances, Hg methylation, nitrification, and genetic samples were collected on the non-trace metal clean ship-owned CTD rosette during the GOA stations. All samples for ambient total mercury (HgT) and MeHg were collected using a trace metal SBE 19plus V2 SeaCAT Profiler (SeaBird) CTD rosette. Hg methylation, nitrification, and genetic samples from the other 13 stations throughout the Bering and

Chukchi Seas were collected utilizing the trace metal CTD. Samples from the trace metal CTD rosette were transferred to acid washed sample bottles (Hammerschmidt and Bowman, 2011) inside a positive-pressure, plastic enclosure (the bubble), constructed at the beginning of the cruise.

Seawater from the GOA HgT analysis was collected in acid-washed 500 mL clear glass bottles and stored until analysis at Wright State University (WSU). Water from the Bering and Chukchi Sea for HgT analysis was collected in acid-washed 250 mL glass bottles and stored until analysis at the University of Connecticut (UConn). All HgT sample bottles were filled to the shoulder to limit air-water interaction. 1.5 L of seawater was collected in acid-washed 2 L fluoropolymer bottles for MeHg analysis from the GOA. Seawater for MeHg analysis from the Bering and Chukchi Sea was collected in 125 mL glass amber bottles. All MeHg samples were stabilized to 1% sulfuric acid (H_2SO_4) by volume with 18 M H_2SO_4 (ACS Grade, Fisher Scientific) and stored in the dark until analysis at WSU and UConn.

Mercury methylation and nitrification rate incubation experiments were carried out shipboard. Seawater samples for Hg rate experiments was collected in acid washed 2 L plastic bottles. Four replicates were collected per sampling station. Seawater samples for nitrification tracer experiments were collected in an acid washed 1 L and 125 mL polycarbonate incubation bottles. Incubation experiments occurred upon sample collection.

Seawater samples for genetic analysis was collected in an acid washed 5-gallon collapsible polyethylene carboy. Using an Eppendorf peristaltic pump, 2 L of sample water was filtered through a 0.22 μM Sterivex filter pack (Millipore). The Sterivexes

were filled with RNAlater (ThermoFisher), stabilizing the nucleic acids until analysis at WSU (Bowman *et al*., 2020).

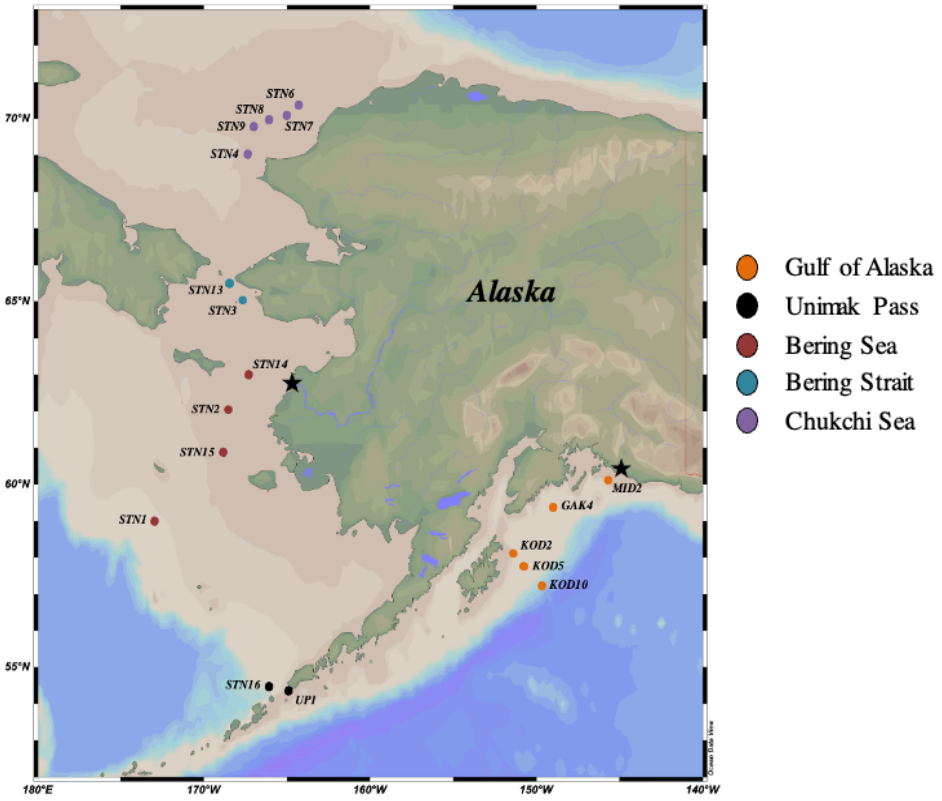

Figure 1. *Map of Gulf of Alaska, Unimak Pass, Bering Sea, Bering Strait and Chukchi Sea 2021 sampling stations. Yukon and Copper River outflows denoted by black stars.*

Mercury Methylation Rate Experiments

On-board dark incubation experiments were carried out with stable Hg isotope additions to quantify Hg methylation and demethylation rates. Upon collection, sample water was amended with 7.5 pM $^{200}Hg^{II}$ (Oak Ridge National Laboratory) and 7.7 pM $CH_3{}^{201}Hg$ by volume. $CH_3{}^{201}Hg$ and $CH_3{}^{199}Hg$ were created prior to the cruise with methyl-cobalamin and inorganic Hg isotopes (Oak Ridge National Laboratory). Final concentrations of isotope additions were quantified during analysis at WSU. Initial sample volume was measured, and samples were placed in a dark incubation chamber at *in situ* temperature (4 ^{o}C). After 24 hours, samples were removed, reduced to 1.5 L and immediately acidified to 1% H_2SO_4 by volume to stop biological transformations. Acidified samples for rate measurements were then amended with 0.04 nM $CH_3{}^{199}Hg$ as a tracer to ensure that no further transformations occurred prior to analysis. Samples were stored in a dark container until analysis at WSU.

Mercury methylation rate samples were analyzed at WSU within 8 months of collection. Prior to analysis, rate samples were neutralized to pH 4.9 $\pm$ 0.2 with 14 M potassium hydroxide (KOH), buffered with 14 mM acetate buffer by volume and amended with 0.1 mL of 2.5% ascorbic acid. Neutralized samples were derivatized with sodium tetraethylborate and purged with Hg-free N_2 gas for 55 mins. During the bubbling process, methylethylmercury was concentrated onto pre-burned Tenax traps and analyzed on an optimized gas chromatography inductively coupled plasma mass spectrometer (GC-ICPMS; Perkin Elmer Elan 9000) with a method detection limit of 0.02% d^{-1} (Hintelmann and Evans, 1997). The peak area for each organic Hg isotope (^{198}Hg, ^{199}Hg, ^{200}Hg, ^{201}Hg, ^{202}Hg) at retention time 2.00 mins was integrated. Ambient Hg standards and

enriched isotope standards were analyzed on both the Tekran and ICP-MS to quantify both concentration and isotope abundance. Mercury methylation and MeHg demethylation rates were calculated using the standard curve (R^2 >0.99), natural abundances, measured isotope ratios, and the reported purity of the standards from ORNL, following matrix methodology (Hintelmann and Evans, 1997).

$$t * k_m = -LN \frac{(I_0 - M_t)}{(I_0)}$$

Mercury methylation was calculated as the $CH_3{}^{200}Hg$ produced from the amended inorganic $^{200}Hg^{II}$. The Hg methylation rate constant (k_m) was calculated from the MeHg concentration (M) at time (t) and the concentration of inorganic Hg amendment (I_0).

$$t * k_l = -LN \frac{(M_0 - M_t)}{(M_0)}$$

Methylmercury demethylation rates were calculated as the $CH_3{}^{201}Hg$ remaining in the sample from the amended $CH_3{}^{201}Hg$. The MeHg demethylation rate constant (k_l) was calculated from the MeHg concentration (M) at time (t) and at time zero (M_0). Both Hg methylation and demethylation are reported as rate potentials.

Nitrification Rate Experiments

The collected 1 L seawater samples were amended with $^{15}NH_4Cl$ to 20 μM and inverted three times. The sample was then transferred into three 125 mL polycarbonate incubation bottles. An initial sample was taken immediately from each incubation

replicate via a 60 mL plastic syringe and filtered through a 0.22 μm filter into one 15 mL polypropylene tube and two 20 mL scintillation vials. An initial control was sampled from the 125 mL unamended seawater sample following the same methodology. Initial samples were frozen upon collection and stored until analysis. The four 125 mL incubation bottles were incubated for 24 hours in the on-board dark incubation chamber at *in situ* temperature. After the 24-hour incubation, the four bottles were removed, final samples from the control and replicates were collected using the same methodology as the initial samples, and samples were frozen until analysis at WSU.

Cadmium (Cd) reductions followed by sodium azide (NaN_3) reductions were completed on each sample to quantify the production of nitrous oxide (N_2O) (Heiss and Fulweiler, 2016; McIlvin and Altabet 2005). To each sample, 100 mg and 6.6 g of dried magnesium and sodium chloride was added respectively and mixed. To complete the Cd reductions, 1 g of activated wet Cd powder was added to each sample and placed on a shaker table for 17 hrs. Samples were centrifuged for 15 min at 1000 rpm to decant the reduced solution. 7.5 mL of supernatant was removed from the centrifuge tubes, transferred to a 12 mL Labco exetainers, and sealed with a single-wadded septa cap. Using a glass syringe with a needle, 0.25 mL of a solution containing 1:1 2 M sodium azide: 20% acetic acid purged with Argon gas was injected into the exetainer septa. Samples were shaken and incubated at 30°C for 1 hr. Following incubation, the reaction was stopped by injecting 0.15 mL of 10 M sodium hydroxide through the exetainer septa with a clean needle and syringe (McIlvin and Altabet, 2005). Exetainers containing the reduced sample were stored upside down and shipped to the University of California - Davis Stable Isotope Facility for analysis of labeled $^{45,46}N_2O$ gas production using an

isotope-ratio mass spectrometer. Incubation samples collected in falcon tubes were thawed and quantified for total NH_4^+ using colorimetric flow-injection analysis (Lachat Quikchem 8500) at WSU. Results from both analyses were used to calculate the $^{15}NH_4^+$ transformation and corrected for NaN_3 reductions using calculations modified from (Heiss and Fulweiler, 2016; Beman *et al.,* 2008; Hampel *et al.,* 2020).

$$NTR = \frac{((^{15}N/^{14}N * [NO_x^-])_{tf} - (^{15}N/^{14}N * [NO_x^-])_{t0})}{\alpha * t}$$

$$where\ \alpha = [^{15}NH_4^+]/([^{15}NH_4^+] + [^{14}NH_4^+])$$

The sum of $^{15}NO_2^-$ and $^{15}NO_3^-$ produced as $^{45}N_2O$ was used to calculate total nitrification rates (NTR), then corrected for efficiency and NH_4 source over the incubation time (tf). Nitrification rates are reported as $^{15}NO_x^-$ produced from amended $^{15}NH_4Cl$.

Ambient Mercury

Total Hg samples from the GOA, analyzed at WSU, were oxidized with bromine monochloride twelve hours prior to analysis (Bloom and Crecelius, 1983). Oxidized samples were neutralized with 0.6 mL of 12% hydroxylamine hydrochloride and inverted three times. Samples were transferred to UConn bubblers and reduced with 100 µL of stannous chloride. Samples were purged for 8 mins with N_2 gas. Gaseous HgT samples were concentrated onto a pre-burned gold traps and analyzed on a Tekran 2500 Cold Vapor Atomic Florescence Spectrophotometer (CVAFS) (Bloom and Crecelius, 1983; Gill and Fitzgerald, 1987). Sample peak area was integrated and HgT concentrations calculated. A standard curve was constructed before every analysis day with a R^2 >0.999. A gas standard was analyzed with a 98-100% recovery to ensure quality control. A

matrix spike with 108% recovery, duplicate sample, and a method blank was also analyzed to ensure quality assurance. MID2 and GAK4 HgT samples were compromised during transport and not reported. HgT samples from the Bering and Chukchi Sea were analyzed using similar methodology at UConn.

Acidified seawater for MeHg analysis from the GOA was neutralized to pH 4.9 $\pm$ 0.2 with 14 M KOH, buffered with 14 mM acetate buffer, and amended with 0.1 mL of 2.5% ascorbic acid prior to analysis (Munson *et al.,* 2014). Samples were transferred into UConn bubblers, derivatized with sodium tetraethylborate, and purged for 9 mins with Hg-free N_2 gas. The gaseous ethylated MeHg sample was concentrated on Tenax traps, separated in gas column, and analyzed on a Tekran 2500 CVAFS (Bloom, 1989, Bowman and Hammerschmidt, 2011). The standard used for analysis was prepared no more than one month prior to analysis and was calibrated using TORT-3 (NRC-CNRC) digestions. A standard curve was created with a R^2 >0.99 prior to each analysis day. A matrix spike with 90-110% recovery, analysis duplicates, continuing calibration verification, and method blank was used to ensure quality assurance and control. Methylmercury samples from the Bering and Chukchi Sea were analyzed using similar methodology at UConn.

Molecular Analysis

Upon arrival to WSU, the Sterivexes were stored at -80 ^{o}C until extraction. DNA was extracted using the DNeasy PowerWater Sterivex Kit (Qiagen) and assessed for quality using 260/280 and 260/230 ratios, with a NanoDrop Microvolume Spectrophotometer (ThermoFisher). Extractions were stored at -18^{o}C until assay. *Nitrospina* specific *hgcA* primers (Table 1), Nitro_SP14_1F and Nitro_SP14_1R,

designed from sequences found in Antarctic Sea ice were used for amplification (Gionfriddo *et al*., 2016). The SP8 sequence, 504 bp, from Gionfriddo *et al*., 2016 was used as a positive control for the real-time polymerase chain reaction (qPCR) assay. A set of seven serial dilutions (10^{-4} – 10^{-10} ng μL^{-1}) were prepared from the SP8 sequence and used to form a standard curve (R^2>0.90). With a reaction volume of 20 μL, the following chemical volumes were used for amplification: 10 μL Luna Universal qPCR Master Mix (New England BioLabs), 1 μL Nitro_SP14_1F and Nitro_SP14_1R, 1 μL of sample (5 ng DNA), diluted SP8, or Nuclease free water, and 7 μL of nuclease free water. Samples were amplified on a Mastercycler ep Realplex2 Real-Time PCR system (Eppendorf) with thermal cycling parameters (outlined in Gionfriddo *et al*., 2016) and a melting curve (Table 1). Amplification efficiency was 95.6%, and sample amplicon concentration was calculated.

$$Gene\ Abundance = \frac{5\ ng * (6.0221 * 10^{23}\ molecules/mol)}{504\ bp *\ 10^{9}\ ng/g\ *\ 650\ g/mol}$$

Nitrospina-specific *hgcA*-like gene abundance was calculated as above and normalized to sample volume.

Table 1. *Nitrospina-specific hgcA-like primers and thermal cycling parameters for qPCR (Gionfriddo et al., 2016).*

Primers	Sequence (5′ - 3′)
Nitro_SP14_1F	GGG GAC TAA TGT CTG GTG TG
Nitro_SP14_1R	AAC AGG GTC TGT TAT TGA CGT
Thermal Cycling Parameters	Initial denaturing (95 °C for 3 min); 15 cycles of denaturing (95 °C for 30 sec), annealing (starting at 65 °C, decreasing by 1 °C every cycle for 45 sec) and elongation (72 °C for 1 min); 20 cycles of denaturing (95 °C for 30 sec), annealing (50 °C for 45 sec) and elongation (72 °C for 1 min); final elongation (72 °C for 5 mins); melting curve; reaction termination (4 °C for 15 min).

III.RESULTS AND DISCUSSION

Physiochemical Oceanography

The sampling depths, targeting the chlorophyll *a* maximum, in the Bering and Chukchi Seas were shallow (48 ± 6 m) compared to the GOA (610 ± 477 m), where sampling depths were deeper and more variable (Table 2). All sampling stations were on the Alaskan continental shelf, except KOD10, which was on the shelf slope in the GOA. At KOD10, DO decreased and salinity increased with depth. Throughout all on-shelf sampling stations, the water column remained oxic. A halocline was observed on the continental shelf across all regions around 25 m depth (Figure 2). All samples were collected in oxic sub-surface, 15-40 m, 300 – 450 μmol kg^{-1} DO (Table 2).

The GOA is heavily influenced by the North Pacific Gyre and Subpolar Gyre which drive the ACC and Alaskan Stream. Melting permafrost and snowpack can release key stored nutrients, such as Fe and Cu, to the Copper River watershed which promotes primary production, such as diatom blooms, in the late spring (Strom *et al*., 2006). Chlorophyll *a* concentrations at the sampling depth across the GOA ranged from 0.3 – 10.1 mg m^{-3} (Table 2). The highest chlorophyll *a* maximum (10.1 mg m^{-3}) was seen at MID2, the Copper River outflow. The Copper River delivers key micro-nutrients such as Fe which aid in autotroph metabolism and assimilation. A distinct low nitrogen (N) and phosphorous (P) signal in the surface waters at the Copper River outflow is seen as the Copper River has lower N and P concentrations than the GOA. Driven by the ACC, these low N and P concentrations at the surface extend west in the GOA. In the GOA, salinity

increased with distance from the coastline, as influence from the Copper River outflow and ACC wanes (Stabeno *et al.,* 2016).

Water flows north via the ACC, Bering Shelf Current and Chukchi Shelf current through the Bering Sea shelf and Bering Strait into the Chukchi Sea (Danielson *et al.,* 2022). These current dynamics are reflected in the salinity profiles (Figure 2). A low salinity signal from the Yukon River in the Shpanberg Strait (27 psu) extended northward into the Bering Strait and Southern Chukchi Sea (31 psu). Decreased temperature was seen at the Yukon River outflow, but overall temperatures decreased with increasing latitude through the Bering and Chukchi Seas (Figure 2). Higher concentrations of chlorophyll *a* and DO were seen in the surface waters in the southern Bering Sea near Unimak Pass (Table 2). This can be attributed to the Aleutian North Slope current and upwelling that resuspends key limited nutrients, such as Fe, to the surface waters of this HNLC system (Danielson *et al.,* 2022; Aguilar-Islas *et al.,* 2007).

Table 2. *Physicochemical factors of sampling stations across the Gulf of Alaska, Unimak Pass, Bering Sea, Bering Strait, and Chukchi Sea.*

Region	Station	Bottom Depth (m)	Sampling Depth (m)	Chl *a* (mg m^{-3})	Temp (°C)	Salinity (psu)	Oxygen (μmol Kg^{-1})
Gulf of Alaska	MID2	118	20	10.1	5.2	31.66	354
	GAK4	200	20	8.8	5.6	31.81	376
	KOD2	125	40	0.3	4.4	31.91	317
	KOD5	88	40	0.3	4.3	32.05	314
	KOD10	2518	20	5.3	5.1	32.40	349
Unimak Pass	UP1	165	40	N.D.	N.D.	N.D.	N.D.
	STN16	540	30	5.4	5.8	32.94	303
Bering Sea	STN1	105	20	5.6	2.7	32.76	364
	STN2	34	15	0.5	-1.6	31.50	339
	STN14	37	15	1.4	0	31.21	402
	STN15	38	15	1.6	2.1	31.36	361
Bering Strait	STN3	33	15	1.6	-1.6	31.47	354
	STN13	54	15	7.8	-0.2	31.78	392
Chukchi Sea	STN4	51	18	0.6	-1.5	31.14	348
	STN5	48	20	0.8	-1.8	33.14	363
	STN6	44	12	8.9	-0.8	32.98	440
	STN7	42	14	5.4	-0.4	33.25	446
	STN9	46	15	5.3	-1.2	32.48	434

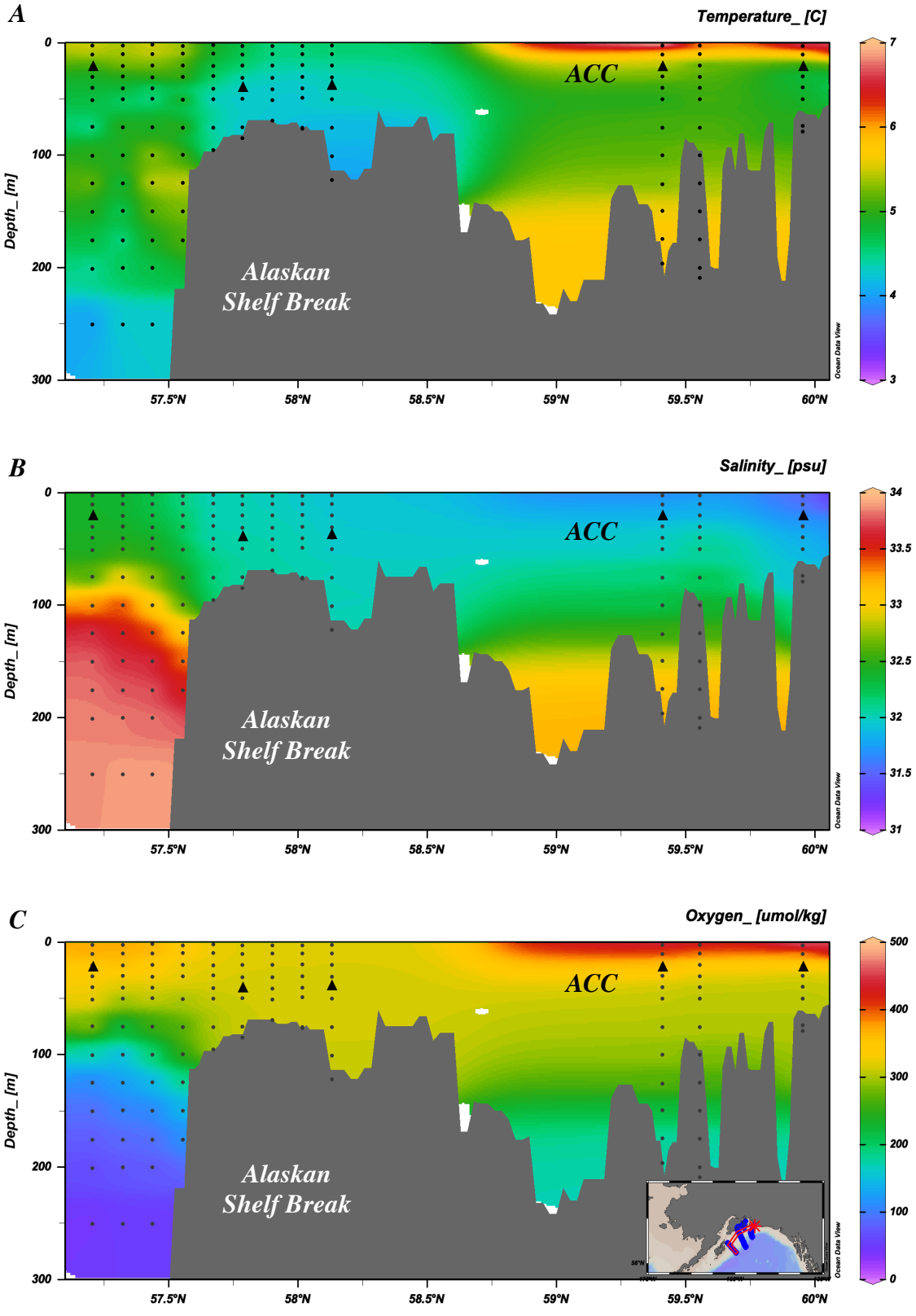
A
Temperature_ [C]
ACC
Alaskan
Shelf Break
Depth_ [m]
0
100
200
300
57.5°N
58°N
58.5°N
59°N
59.5°N
60°N
7
6
5
4
3
Ocean Data View
B
Salinity_ [psu]
ACC
Alaskan
Shelf Break
Depth_ [m]
34
33.5
33
32.5
32
31.5
31
Ocean Data View
C
Oxygen_ [umol/kg]
ACC
Alaskan
Shelf Break
Depth_ [m]
500
400
300
200
100
0
Ocean Data View

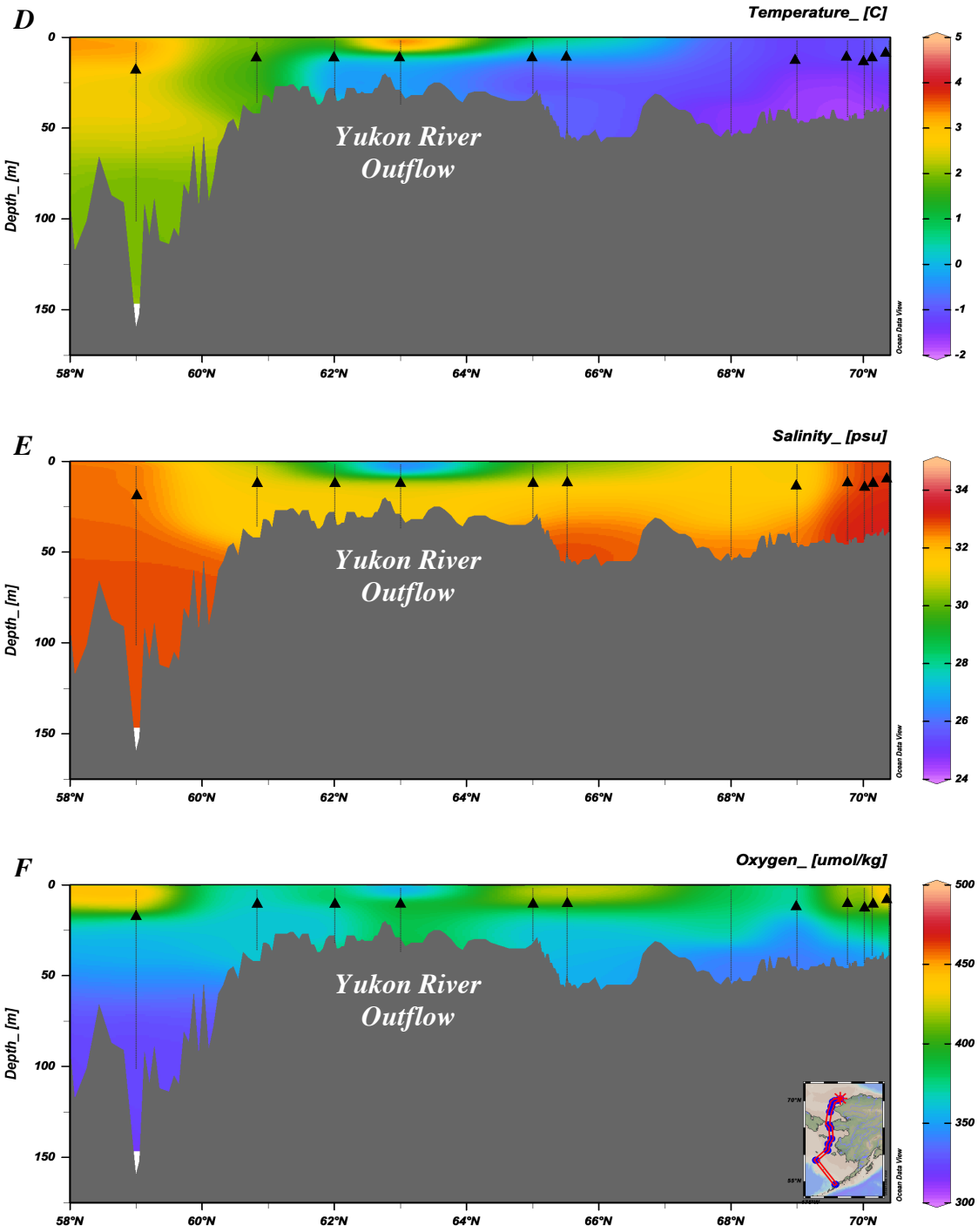

Figure 2. *Depth profiles showing temperature, salinity, and oxygen across the Northern Gulf of Alaska (A-C) and the Bering and Chukchi Seas (D-F). Triangles denote rate sampling depth. Points and lines denote CTD cast.*

Ambient Mercury

Ambient HgT concentrations across all regions ranged 0.17 pM to 2.03 pM HgT. These findings were consistent with previous filtered measurements on the U.S. GEOTRACES: GN01 transect (0.86 $\pm$ 0.45 pM HgT) and unfiltered measurements west of Kodiak Island in the GOA (1.26 $\pm$ 0.32 pM HgT) (Agather *et al.,* 2019; Sunderland *et al.,* 2009). Total Hg concentrations did not significantly differ between sub-Arctic regions (Table 3). The western GOA had the highest HgT concentrations (1.83 $\pm$ 0.12 pM HgT). Further investigation of Hg transport and loading by the Copper River should be completed across the GOA. In the Bering Sea, Bering Strait, and Chukchi Sea HgT concentrations decreased at the chlorophyll *a* maximum with increased latitude (Table 3). Full HgT depth profiles were assessed and interpreted in Inman *et al*. (2022).

Across the sub-Arctic regions, ambient unfiltered MeHg concentrations at the chlorophyll *a* maximum ranged 1.4 fM to 37 fM MeHg. This is lower than previous filtered measurements in the Arctic (Agather *et al.,* 2019; Sunderland *et al.,* 2009), suggesting that the chlorophyll *a* maximum may not be the MeHg maximum at the sampling stations. Further investigation of full water column MeHg profiles should be completed. The Bering Sea had significantly lower MeHg concentrations than the GOA, Bering Strait, and Chukchi Sea (one-way ANOVA: $p<0.05$). This significant decrease in the Bering Sea isn't seen in the ambient HgT and Hg methylation rate potential measurements relative to other regions (Table 3). Ambient MeHg concentrations in the GOA were only reported for one station, KOD10 which is located on the shelf slope. All other stations (MID2, GAK4, KOD2 and KOD5), located on the Alaskan shelf, contained

reactive species that interacted with the pyrolizer in the CVAFS yielding a low peak separation (personal communication: Yipeng He and Robert Mason; Table S1).

The percentage of MeHg in HgT species in the water column was consistent across the GOA (1.4 %), Bering Sea (1.3 $\pm$ 0.6 %) and Chukchi Sea (2.8 $\pm$ 0.8 %), but higher at the single station in the Bering Strait, STN13, (6.5 %) (Table 3). The higher percentage of MeHg in the Bering Strait is seen in the ambient MeHg measurement (37.1 fM MeHg), but not the specific Hg methylation rate (0.008 d^{-1}). This suggests MeHg production at the time of sample collection in the Bering Strait might be occurring at an alternate depth than the chlorophyll *a* maximum, such as the benthos. Higher ambient MeHg concentrations at STN13 could be attributed to water column mixing, re-suspension of MeHg produced in sediments and increased MeHg demethylation, but replication is necessary to better understand the mechanisms.

Table 3. *Mean ambient mercury concentrations with standard error across five regions: Gulf of Alaska, Unimak Pass, Bering Sea, Bering Strait, and Chukchi Sea.*

Region	Depth (m)	HgT (pM)	MeHg (fM)	MeHg:HgT (%)
Gulf of Alaska	15 - 40	1.83 $\pm$ 0.12	21.4	1.4
Unimak Pass	30 - 40	N.D.	N.D.	N.D.
Bering Sea	15 - 20	0.92 $\pm$ 0.32	8.9 $\pm$ 4.9	1.3 $\pm$ 0.6
Bering Strait	15	1.09 $\pm$ 0.48	37.1	6.5
Chukchi Sea	12 - 20	0.75 $\pm$ 0.13	20.9 $\pm$ 6.9	2.8 $\pm$ 0.8

Mercury Transformations

In situ Hg methylation occurred at all stations (0.003 – 0.008 d^{-1}). Mercury methylation rate potentials across all regions were comparable with previous measurements from the Arctic (0.006 – 0.007 d^{-1}), Mediterranean Sea (0.003 – 0.063 d^{-1}) and the central Pacific Ocean at the chlorophyll *a* maximum (0.004 – 0.017 d^{-1}) (Lehnherr *et al.,* 2011; Monperrus *et al.,* 2007; Munson *et al.,* 2018). Within each region, the Hg methylation rate potentials were variable (Table 4). Variability within each region is attributed to temporal and spatial heterogeneity between sampling stations impacting particle and nutrient distribution from differing current dynamics (Strom *et al.,* 2006). Differing assemblages of Hg methylating bacteria, Hg availability, and MeHg demethylation rates also contribute to the variability of Hg methylation rate potentials within each sampled sub-Arctic region. The highest Hg methylation rate potentials were measured at Unimak Pass (one-way ANOVA: $p<0.05$; Table 4). Higher concentration of particles from upwelling at Unimak Pass provide a substrate and microhabitat for Hg methylating anaerobic bacteria explaining the high Hg methylation rate potentials (Swift and Aagaard, 1976; Capo *et al.,* in review; Ortiz *et al.,* 2015; Bowman *et al.,* 2016). The GOA had the lowest Hg methylation rate potentials (Table 4). The samples for incubation experiments in the GOA were collected in the early spring season when productivity and snowmelt is lower (Strom *et al.,* 2006). Across all regions, correlations between Hg methylation rate potentials and DO, ambient Hg, ambient NH_4^+, salinity, and temperature were weak and not significant. Using the mean Hg methylation specific rates and ambient inorganic Hg concentrations, the gross potential *in situ* MeHg production over 24 hours can be calculated for the GOA (4.0 fM d^{-1}), Bering Sea (3.5 fM d^{-1}), Bering Strait (4.4 fM

d^{-1}), and Chukchi Sea (4.5 fM d^{-1}). These estimates are lower than the measured ambient MeHg concentrations (Table 4), but when compounded over a two-week period measured MeHg production exceeds ambient water column measurements. Mercury methylation follows Michaelis-Menten kinetics, meaning this transformation is substrate limited (Date *et al.,* 2019). With lower ambient Hg^{II} inputs than amended $^{200}Hg^{II}$ the *in situ* specific Hg methylation rates are predicted to be lower. The difference between predicted MeHg formation over a two-week period and ambient MeHg concentrations is most likely attributed to MeHg demethylation in the surface waters and mixing throughout the Bering Strait and Chukchi Sea (Wang *et al.,* 2018; DiMento and Mason, 2017; Munson *et al.,* 2018).

Methylmercury demethylation rate potentials were not reported as the rates were inflated due to instantaneous demethylation upon amendment (Munson *et al.,* 2018). This conclusion is based on the finding that $CH_3{}^{199}Hg$ tracer amendment after the incubations was not fully recovered (1-6%), suggesting that this loss was from abiotic rather than microbial processes upon its addition. When compared to the MeHg demethylation rate potential percentages (87-99%) the low $CH_3{}^{199}Hg$ recovery is attributed to instantaneous demethylation (Munson *et al.,* 2018). For future Hg rate potential experiments, a time integrated approach should be taken to eliminate this issue.

Table 4. *Mean Nitrospina-specific hgcA-like gene abundance and rate potentials with standard error across five regions: Gulf of Alaska, Unimak Pass, Bering Sea, Bering Strait, and Chukchi Sea.*

Region	Hg Methylation (10^{-3} d^{-1})	Hg Methylation (10^{-2} pM d^{-1})	Nitrification (nM d^{-1})	Gene Abundance (copies mL^{-1})
Gulf of Alaska	2.8 $\pm$ 0.6	1.8 $\pm$ 0.4	1.3 $\pm$ 0.6	2023 $\pm$ 957
Unimak Pass	8.3 $\pm$ 2.5	5.9 $\pm$ 1.9	N.D.	236
Bering Sea	4.3 $\pm$ 1.3	2.3 $\pm$ 0.5	1.7 $\pm$ 1.2	1895 $\pm$ 1461
Bering Strait	5.3 $\pm$ 2.6	4.4 $\pm$ 1.2	0.5 $\pm$ 0.4	2914 $\pm$ 278
Chukchi Sea	5.8 $\pm$ 1.7	4.2 $\pm$ 1.2	1.9 $\pm$ 0.8	1879 $\pm$ 784

Nitrification

Nitrification rate potentials did not vary significantly across sub-arctic regions (Table 3). Nitrification rate potentials across all sub-polar regions (0.5 – 2.0 nM d^{-1}) were on the lower end of the range of measurements in the upper 50 m in the North Pacific and Sub-Arctic (0 – 40 nM d^{-1}) (Shiozaki *et al.,* 2016), but similar to measurements at deeper depths, 100 – 200 m, in other oligotrophic regions such as the Sargasso Sea (2.0 + 0.1 nM d^{-1}) (Newell *et al.,* 2013). The global estimate for marine specific nitrification rates, 0.016 d^{-1}, is higher than the mean specific nitrification rates across all regions in this study of 7.2 x 10^{-5} d^{-1}. The low mean specific nitrification rate in this study may be driven by low temperature or a low saturation concentration despite the high $^{15}NH_4Cl$ amendment.

Nitrification rate potentials within each sub-polar region were variable (Table 4). In the Chukchi Sea (1.9 $\pm$ 0.8 nM d^{-1}), nitrification rate potentials were consistent with previous measurements in the surface waters within the Chukchi and Beaufort Seas in Shiozaki *et al.,* (2019) (< 0.27 nM d^{-1}). Nitrification rate experiments were not conducted at Unimak Pass. Future research could confirm the hypothesis that Unimak Pass would have a higher apparent nitrification rate as the ACC and upwelling currents would provide copper and iron, which are metal centers for enzymes involved in nitrification and metabolism, as well as re-mineralized ammonium.

Overall, nitrification rates were low when compared to equatorial regions, which was expected as the sub-Arctic is limited by micro-nutrients such as Fe and Cu (Aguilar-Islas *et al.,* 2007). Substrate availability (NH_4^+), light transmittance and pH are thought to be the main drivers in nitrification rates throughout the water column in the Arctic (Shiozaki *et al.,* 2016; Shiozaki *et al.,* 2019). It is likely that at the chlorophyll *a*

maximum, competition between microbes and plankton taking up various forms of N are driving the lower nitrification rates in this study. The NO_2^- maximum, where high nitrification rates are typically highest, resides under the chlorophyll *a* maximum where biological activity, and thus competition, is not as great (Lomas and Lipschultz, 2006). The location of the NO_2^- maximum at the base of the euphotic zone may also be driven by the fact that many known NH_3 oxidizing bacteria have been shown to be photo-inhibited, resulting in higher nitrification rates with reduced light attenuation (Merbt *et al*., 2012; Horrigan and Springer, 1990). Previous studies in the North Pacific and Arctic Ocean show nitrification maxima occurring below the chlorophyll *a* maximum under <1% PAR (Grundle *et al*., 2013; Shiozaki *et al*., 2016; Shiozaki *et al*., 2019). It cannot be concluded whether the NO_2^- maximum differs from the chlorophyll *a* maximum across sampling stations despite >1 – 9 % PAR at sampling depths. The nitrification rate potentials measured at the chlorophyll *a* maximum across all sub-polar marine regions reported in this study are not expected to reflect the highest nitrification rates in the water column. Future research should investigate nitrification throughout the water column in these sub-polar regions to better understand NO_3^- production.

An understanding of nitrification in the Arctic is important as with decreasing ocean pH and increasing temperatures from global warming, nitrification rates are predicted to overall decrease by 3 – 44 % (Beman *et al*., 2011). With over half of the assimilated NO_3^- originating from nitrification, this substantial decrease in NO_3^- production, particularly in ice covered regions, could vastly alter the Arctic food web (Yool *et al*., 2007; Hutchins and Fu, 2017; Shiozaki *et al*., 2019).

Mercury Methylation and Nitrification

A significant positive linear relationship between nitrification and Hg methylation rate potentials across all stations suggests a possible link between these two processes at the chlorophyll *a* maximum across the four sub-Arctic regions (linear regression: $p<0.05$; Figure 3). The linear regression slope between nitrification and Hg methylation rate potentials across all regions in the sub-Arctic ($m = 0.0087$) is the same order of magnitude as previous findings in the Amazon River Plume ($m = 0.0028$) (Starr *et al.*, in review; Figure 3). The difference in slope and y-intercepts may be attributed to differing NH_3 oxidizing bacteria and archaea activities, substrate availability, and microbial assemblages, including nitrifier community structure.

STN13 in the Bering Strait had a higher Hg methylation rate potential compared to the nitrification rate potential (0.17, 8.0) (Figure 3). Chlorophyll *a* concentrations at STN13 were four times higher than those of STN3, the other station within the Bering Strait sampled 12 days prior to STN13 (Table 2; Table S1). Higher chlorophyll *a* concentrations suggest a general increase in microbial activity. Data from the USGS Yukon River Pilot Station show little change in Yukon River discharge throughout the 12-day period between sampling, suggesting riverine inputs were not the main driver in differing rate potentials. First year ice melt could influence the rate potentials between the two stations in the Bering Strait. The reduction in ice cover could change current dynamics driven by winds promoting water column mixing and re-suspension of particles inhabited by Hg methylators. Although these are potential reasons for why STN13 had a higher Hg methylation rate potential compared to the nitrification rate potential, more samples would need to be collected to draw any conclusions.

MID2, in the GOA near the Copper River outflow, had a higher nitrification rate potential compared to the Hg methylation rate potential. This higher nitrification rate potential can be attributed to micro-nutrient loading, such as NH_4^+ and Cu, from the river discharge and differing communities of nitrifiers that can withstand estuarian salinity dynamics (Bernhard *et al.,* 2010). Lower substrate availability for Hg methylation from Copper River discharge containing particle bound Hg^{II}, from terrestrial dissolved organic matter, could also be driving lower Hg methylation relative to nitrification rate potentials in the GOA. This suggests that increased snowpack melt and Copper River discharge in late summer could alter allochthonous organic matter inputs and Hg^{II} loading, impacting Hg methylation rate potentials in the GOA. Further research should be completed investigating sources and sinks, such as particle scavenging, of Hg in the GOA and Copper River throughout the summer. Likely due to the temporal and spatial differences between each station, there was higher variability in the spread of the linear regression than previous measurements in the Amazon River Plume ($R^2 = 0.78$; Figure 3; Starr *et al.,* in review).

Across all regions, the stations in Chukchi Sea were sampled within the shortest time period (6-days) and across the smallest distance (110 miles) (Table S1). The correlation between Hg methylation and nitrification rate potentials in the Chukchi sea was significant ($R^2 = 0.99$, $p<0.001$; Figure 4), but had a higher slope ($m = 0.0154$) than the linear regression across all regions and the Amazon River plume. This tighter fit can likely be attributed to lack of spatial and temporal variability of the stations. Although the correlation between nitrification and Hg methylation rate potentials were significant, it cannot be concluded that nitrification rates are driving Hg methylation rates throughout

these sub-polar regions, as the functionality of *Nitrospina*-specific *hgcA*-like genes have not yet been confirmed. Other biogeochemical processes could be a proxy for nitrification and thus Hg methylation in this region.

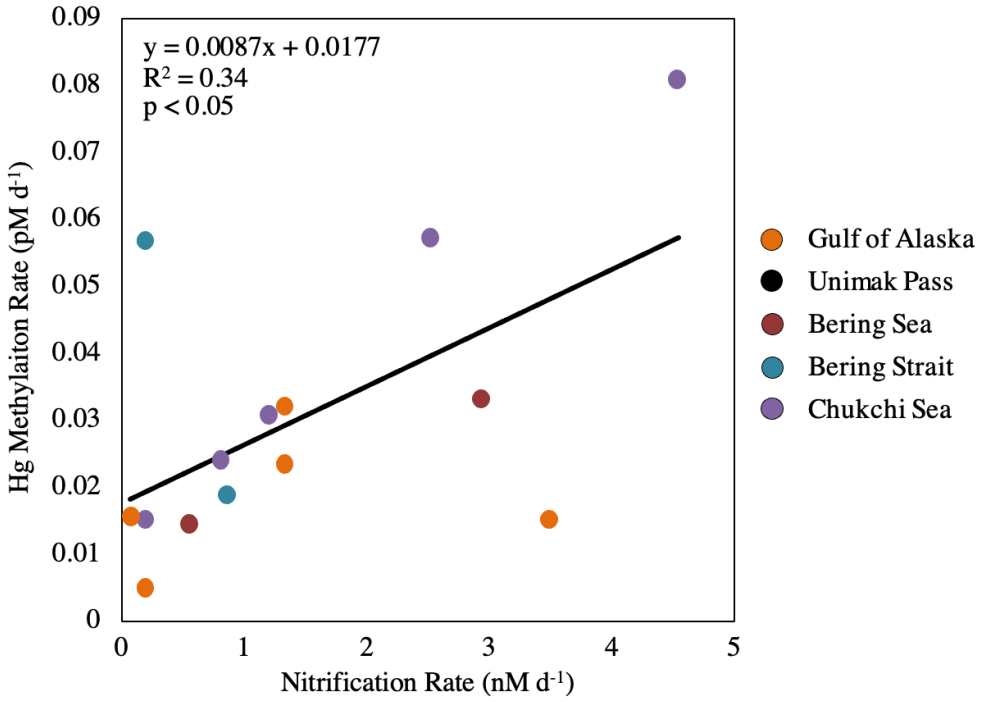

Figure 3. *Linear regression between nitrification and mercury methylation rate potentials across five sub-Arctic regions ($p < 0.05$, $y = 0.0087x + 0.0177$).*

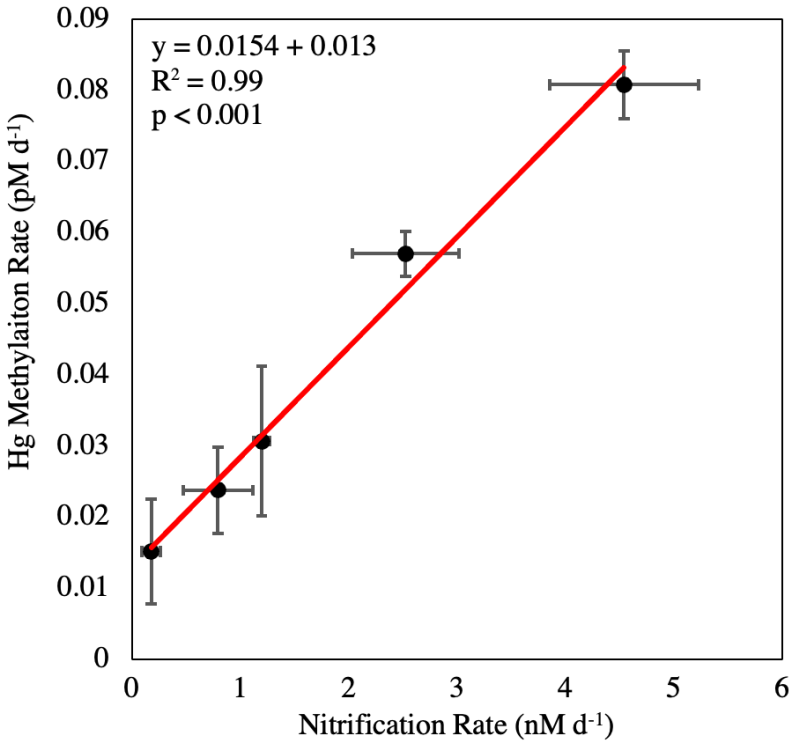

Figure 4. *Linear regression between nitrification and mercury methylation rate potentials in the Chukchi Sea with standard errors ($p < 0.001$, $y = 0.0154x + 0.013$).*

Genetics

Nitrospina-specific *hgcA*-like genes were found across all stations at varying abundances. The Bering Strait had the highest average gene copy numbers (2914 copies mL^{-1}) compared to the GOA (2023 copies mL^{-1}), Bering Sea (1895 copies mL^{-1}), and Chukchi Sea (1879 copies mL^{-1}). Unimak Pass had the lowest gene abundance (236 copies mL^{-1}), which was surprising as Unimak Pass had the highest Hg methylation rate potentials (Table 4), but nitrification was not measured at this station. Mercury methylation in the sub-surface at Unimak Pass can likely be attributed to differing anaerobic Hg methylating microbial communities inhabiting anoxic re-suspended particle micro-environments (Capo *et al.,* in review), which would be dominated by anaerobic bacteria. It is hypothesized that anaerobic Hg methylating microbes inhabit falling or suspended particles throughout all regions and re-suspended particles in the well mixed, shallow Bering Strait and Chukchi Sea (Capo *et al.,* in review; Ortiz *et al.,* 2015). Previous studies have found anaerobic Hg methylating microbes such as *Desulfobacteraceae* and *Methanomassiliicoccus* throughout the Bering Sea, Chukchi Sea, and Arctic Ocean water column (Bowman *et al.,* 2020). Across all regions and within each region there was not a correlation between *Nitrospina*-specific *hgcA*-like genes and Hg methylation rate potentials. These *Nitrospina hgcA*-like sequences only show gene presence, not enzyme function. Starr *et al*. (in review) found a positive correlation between *Nitrospina*-specific *16S* expression and Hg methylation rate potentials, but *Nitrospina*-specific *hgcA*-like genetics were not investigated. Presumably, if *Nitospina*

hgcA-like genes are functional, then *Nitrospina*-specific *hgcA*-like transcript abundance would positively correlate with Hg methylation rate potentials across all stations.

Knowledge of Hgc-containing microorganisms continues to grow as *hgcAB* genes are hypothesized to be horizontally transferred (Cooper *et al.,* 2020; Gionfriddo *et al.,* 2020). Each discovery broadens understanding of environments and niches capable of Hg methylation. As the list of putative and confirmed Hg methylators grows, further metagenomic analysis should be completed to access the entire Hg methylating microbial community as it is likely that *Nitrospina* isn't the only putative Hg methylator present in these regions. We targeted *Nitrospina*, as they have been found across all ocean basins, including the Arctic. There is still no conclusive evidence to suggest that the *Nitrospina*-specific *hgcA*-like gene fragments found across the five sub-Arctic regions have functional cobalamin transfer genes that facilitate Hg methylation. It is speculated that Hg methylation can be completed without *hgcB* to facilitate the reduction step, but this has not been demonstrated. *In situ* Hg methylation rate experiments should be completed with cultured *Nitrospina* to confirm Hg methylating capabilities.

IV. CONCLUSION

The link between Hg methylation and nitrification at the chlorophyll *a* maximum across these sub-Arctic regions suggests a possible aerobic pathway for Hg methylation. The similarity between this relationship in the sub-Arctic and Amazon River Plume further supports the hypothesis that nitrification and biotic Hg methylation are linked in the oxic ocean sub-surface. With *Nitrospina hgcA*-like metagenomes recovered across all ocean basins (Villar *et al.,* 2020; Bowman *et al.,* 2020; Tada *et al.,* 2021), *Nitrospina* could be a major pathway for MeHg formation in the oxic ocean sub-surface if the conserved region of *hgcA* is functional. If *Nitrospina*-specific *hgcA*-like genes are functional, models utilizing current global specific nitrification rate estimates and *Nitrospina hgcA*-like amino acid sequence recoveries could predict global Hg methylation rate potentials in the ocean sub-surface. Until *Nitrospina*'s Hg methylating capabilities are confirmed in culture, conclusions regarding Hg methylation by *Nitrospina* cannot be made. If *Nitrospina* cannot facilitate Hg methylation, the link between Hg methylation and nitrification should be further investigated to further understand their correlation. The discovery of *Nitrospina*-specific *hgcA*-like genes in 2016 suggests that future research should focus on other putative aerobic marine Hg methylating pathways (Gionfriddo *et al.,* 2016). *In situ* Hg methylation measurements have been made across oxic regions in the Arctic, Central Pacific, and Equatorial Atlantic, but more measurements with metagenomic analysis should be completed to further support the methylation pathway (this study, Lehnherr *et al.,* 2011; Munson *et al.,*

2018; Starr *et al*., in review). With MeHg production in the Arctic remaining a prominent area of interest, further research should be completed investigating major pathways of MeHg production in the Arctic, including particle microenvironments or benthic production and re-suspension and re-mineralization. As this study reports the first measurements of ambient Hg and *in situ* Hg methylation along the ACC in the northern GOA, full depth profiles including Hg bound to particulates should be investigated to discern sources such as the Copper River, sinks, and the fate of Hg species in the GOA. This study and future research will aid in the understanding of Hg cycling in the ocean sub-surface, particularly the Arctic where high MeHg concentrations in marine predators is of growing concern for their health and those who consume them.

V. REFERENCES

Agather, A.M., K.L. Bowman, C.H. Lamborg and C.R. Hammerschmidt. 2019. Distribution of mercury species in the Western Arctic Ocean (U.S. GEOTRACES GN01). *Marine Chemistry*, 216(20).

Aguilar-Islas, A.M., M.P. Hurst, K.N. Buck, B. Sohst, G.J. Smith, M.C. Lohan and K.W. Bruland. 2007. Micro- and macronutrients in the southeastern Bering Sea: Insight into iron-replete and iron-depleted regimes. *Progress in Oceanography*, 73(2): 99-126.

AMAP. 2021. AMAP Assessment 2021: human health in the Arctic. *Arctic Monitoring and Assessment Programme, Tromsø, Norway*.

Ariya, P.A., A.P. Dastoor, M. Amyot, W.H. Schroeder, L. Barrie, K. Anlauf, F. Raofie, A. Ryzhkov, D. Davignon, J. Lalonde and A. Steffen. 2004. The Arctic: a sink for mercury. *Chemical and Physical Meteorology*, 56(5).

Beckmen, K.B., L.K. Duffy, X. Zhang and K.W. Pitcher. 2002. Mercury concentrations is the fur of Steller sea lions and northern fur seals from Alaska. *Marine Pollution Bulletin*, 44(10): 1130-1135.

Beman, J.M., B.N. Popp and C.A. Francis. 2008. Molecular and biogeochemical evidence for ammonia oxidation by marine *Crenarchaeota* in the Gulf of California. *The ISME Journal*, 2: 429-441.

Benoit, J.M., C.C. Gilmour, A. Heyes, R.P. Mason and C.L. Miller. 2003. Geochemical and biological controls over methylmercury production and degradation in aquatic ecosystems. *Biogeochemistry of Environmentally Important Trace Elements*.

Bernhard, A.E., Z.C. Landry, A. Blevins, J.R. de la Torre, A.E. Giblin and D.A. Stahl. 2010. Abundance of ammonia-oxidizing *Archaea* and *Bacteria* along an estuarine salinity gradient in relation to potential nitrification rates. *Applied and Environmental Microbiology*, 76(4).

Bloom, N.S. 1989. Determination of picogram levels of methylmercury by aqueous phase ethylation, followed by cryogenic gas chromatography with cold vapor atomic fluorescence detection. *Canadian Journal of Fisheries and Aquatic Sciences*.

Bloom, N.S. and Crecelius, E.A. 1983. Determination of mercury in seawater at sub-nanogram per liter levels. *Marine Chemistry*, 14(1): 49-59.

Bowman, K.L. and Hammerschmidt, C.R. 2011. Extraction of monomethylmercury from seawater for low-femtomolar determination. *Limnology and Oceanography: Methods*, 9(4): 121-128.

Bowman, K.L., C.H. Lamborg and A.M. Agather. 2020. A global perspective on mercury cycling in the ocean. *Science of The Total Environment*, 710.

Boyd, P.W., C.S. Law, C.S. Wong, Y. Nojiri, A. Tsuda, M. Levasseur, S. Takeda, R. Rivkin, P.J. Harrison, R. Strzepek, J. Gower, R.M. McKay, E. Abraham, M. Arychuk, J. Barwell-Clarke, W. Crawford, D. Crawford, M. Hale, K. Harada, K. Johnson, H. Kiyosawa, I. Kudo, A. Marchetti, W. Miller, J. Needoba, J. Nishioka, H. Ogawa, J. Page, M. Robert, H. Saito, A. Sastri, N. Sherry, T. Soutar, N. Sutherland, Y. Taira, F. Whitney, S.E. Wong and T. Yoshmura. 2004. The decline and fate of an iron-induced subarctic phytoplankton bloom. *Nature*, 428: 549-553.

Brabets, T.P., B. Wang and R.H. Meade. 2000. Environmental and hydrologic overview of the Yukon River Basin, Alaska and Canada. *Water-Resources Investigations Report 99-4204*.

Capo, E., A.G. Bravo, A.L. Sørensen, S. Bertilsson, J. Pinhassi, C. Feng, A.F. Andersson, M. Buck and E. Björn. *In review*. Marine snow as a habitat for microbial mercury methylators in the Baltic Sea. *pre-print*

Celo, V., D.R.S. Lean and S.L. Scott. 2006. Abiotic methylation of mercury in the aquatic environment. *Science of The Total Environment*, 368(1): 126-137.

Christensen, G.A., C.M. Gionfriddo, A.J. King, J.G. Moberly, C.L. Miller, A.C. Somenahally, S.J. Callister, H. Brewer, M. Podar, S.D. Brown, A.V. Palumbo, C.C. Brandt, A.M. Wymore, S.C. Brooks, C. Hwang, M.W. Fields, J.D. Wall, C.C. Gilmour and D.A. Elias. 2019. Determining the reliability of measuring mercury cycling gene abundance with correlations with mercury and methylmercury concentrations. *Environmental Science and Technology*, 53(15): 8649-8663.

Clarkson, T.W. and Magos, L. 2008. The toxicology of mercury and its chemical compounds. *Critical Reviews in Toxicology*, 8.

Cooper, C.J., K. Zheng, K.W. Rush, A. Johs, B.C. Sanders, G.A. Pavlopoulos, N.C. Kyrpides, M. Podar, S. Ovchinnikov, S.W. Ragsdale and J.M. Parks. 2020. Structure determination of the HgcAB complex using metagenome sequence data: insights into microbial mercury methylation. *Communications Biology*, 3.

Danielson, S.L., J.M. Grebmeier, K. Iken, C. Berchok, L. Britt, K.H. Dunton, L. Eisner, E.V. Farley, A. Fujiwara, D.D.W. Hauser, M. Itoh, T. Kikuchi, S. Kotwicki, K.J. Kuletz, C.W. Mordy, S. Nishino, C. Peralta-Ferriz, R.S. Pickart, P.S. Stabeno, K.M. Stafford, A.V. Whiting and R. Woodgate. 2022. Monitoring Alaskan Arctic Shelf ecosystems through collaborative observation networks. *Oceanography*, 35(2).

Dastoor, A., H. Angot, J. Bieser, J.H. Christensen, T.A. Douglas, L. Heimbürger-Boavida, M. Jiskra, R.P. Mason, D.S. McLagan, D. Obrist, P.M. Outridge, M.V. Petrova, A. Ryjkov, K.A. St. Pierre, A.T. Schartup, A.L. Sørensen, K. Toyota, O. Travnikov, S.J. Wilson and C. Zdanowicz. 2022. Arctic mercury cycling. *Nature Reviews Earth and Environment*, 3: 270-286.

Date, S.S., J.M. Parks, K.W. Rush, J.D. Wall, S.W. Ragsdale and A. Johs. 2019. Kinetics of enzymatic mercury methylation at nanomolar concentrations catalyzed by HgcAB. *Applied and Environmental Microbiology*, 85.

Delwiche, C.C. 1970. The nitrogen cycle. *Scientific American*, 233(3): 136-147.

Dietz, R., P.M. Outridge and K.A. Hobson. 2009. Anthropogenic contributions to mercury levels in present-day Arctic animals – A review. *Science of The Total Environment*, 407(24): 6120-6131.

Dietz, R., C. Sonne, N. Basu, B. Braune, T. O'Hara, R.J. Letcher, T. Scheuhammer, M. Anderson, C. Andreasen, D. Andriashek, G. Asmund, A. Aubail, H. Baagoe, E.W. Born, H.M. Chan, A.E. Derocher, P. Grandjean, K. Knott and J. Aars. 2013. What are the toxicological effects of mercury in biota? *Science in The Total Environment*, 443(15): 775-790.

DiMento, B.P. and Mason, R.P. 2017. Factors controlling the photochemical degradation of methylmercury in coastal and oceanic waters. *Marine Chemistry*, 196: 116-125.

Fitzgerald, W.F., C.H. Lamborg and C.R. Hammerschmidt. 2007. Marine biogeochemical cycling of mercury. *Chemical Reviews*, 107(2): 641-662.

Gill, G.A. and Fitzgerald, W.F. 1987. Picomolar mercury measurements in seawater and other materials using stannous chloride reduction and two-stage gold amalgamation with gas phase detection. *Marine Chemistry*, 20(3): 227-243.

Gilmour, C.C., M. Podar, A.L. Bullock, A.M. Graham, S.D. Brown, A.C. Somenahally, A. Johs, R.A. Hurt, K.L. Bailey and D.A. Elias. 2013. Mercury methylation by novel microorganisms from new environments. *Environmental Science and Technology*, 47(20): 11810-11820.

Gionfriddo, C.M., M.T. Tate, R.R. Wick, M.B. Schultz, A. Zemla, M.P. Thelen, R. Schofield, D.P. Krabbenhoft, K.E. Holt and J.W. Moreau. 2016. Microbial mercury methylation in Antarctic sea ice. *Nature Microbiology*, 1.

Gionfriddo, C.M., M.B. Stott, J.F. Power, J.M. Ogorek, D.P. Krabbenhoft, R. Wick, K. Holt, L. Chen, B.C. Thomas, J.F. Banfield and J.W. Moreau. 2020. Genome-resolved metagenomics and detailed geochemical speciation analyses yield new insights into microbial mercury cycling in geothermal springs. *Applied Environmental Microbiology*, 86(15).

Gionfriddo, C.M., E. Capo, B. Peterson, H. Lin, D. Jones, A. Bravo, S. Bertilsson, J. Moreau, K. McMahon, D. Elias and C. Gilmour. 2021. Hg-MATE-Db.v1.01142021: Hg-cycling microorganisms in aquatic and terrestrial ecosystems database.

Grundle, D.S., K. Juniper and K.E. Giesbrecht. 2013. Euphotic zone nitrification in the NE subarctic Pacific: implications for measurements of new production. *Marine Chemistry*, 155: 113-123.

Hammerschmidt, C.R. and Fitzgerald, W.F. 2006. Methylmercury in freshwater fish linked to atmospheric mercury deposition. *Environmental Science and Technology*, 40(24): 7764-7770.

Hammerschmidt, C.R., K.L. Bowman, M.D. Tabatchnick and C.H. Lamborg. 2011. Storage bottles material and cleaning for determination of total mercury in seawater. *Limnology and Oceanography: Methods,* 9(10): 426-431.

Hampel, J.J., M.J. McCarthy, S.L. Aalto and S.E. Newell. 2020. Hurricane disturbance stimulated nitrification and altered ammonia oxidizer community structure in Lake Okeechobee and St. Lucie Estuary (Florida). *Frontiers in Microbiology*.

Heimbürger, L., J.E. Sonke, D. Cossa, D. Point, C. Lagane, L. Laffont, B.T. Galfond, M. Nicolaus, B. Rabe and M. Rutgers van der Loeff. 2015. Shallow methylmercury production in the marginal sea ice zone of the central Arctic Ocean. *Scientific Reports*, 5.

Hess, E.M. and Fulweiler, R.W. 2016. Coastal water column ammonium and citrate oxidation are decoupled in summer. *Estuarine, Coastal and Shelf Science*, 178: 110-119.

Hintelmann, H. and Evans, R.D. 1997. Application of stable isotopes in environmental tracer studies – Measurement of monomethylmercury by isotope dilution ICP-MS and detection of species transformation. *Fresenius' Journal of Analytical Chemistry*, 358: 378-385.

Horowitz, H.M., D.J. Jacob, H.M. Amos, D.G. Streets and E.M. Sunderland. 2014. *Environmental Science and Technology*, 48(17): 10242-10250.

Horrigan, S.G. and Springer, A.L. 1990. Oceanic and estuarine ammonium oxidation: effects of light. *Limnology and Oceanography*, 35(2): 479-482.

Hutchins, D.A. and Fu, F. 2017. Microorganisms and ocean global change. *Nature Microbiology*, 2.

Inman, H., Y. He and R.P. Mason. 2022. Speciation and distribution of mercury in the water column and sediments of the Bering and Chukchi Seas. ASLO: Ocean Science Meeting 2022.

Jonsson, S., M.G.N. Mastomonaco, K. Gardfeldt and R.P. Mason. 2022. Distribution of total mercury and methylated mercury species in Central Arctic Ocean water and ice. *Marine Chemistry*, 242.

Kelley, J.J., L.L. Longerich and D.W. Hood. 1971. Effect of upwelling, mixing, and high primary productivity on CO_2 concentrations in surface waters of the Bering Sea. *Journal of Geophysical Research*, 76(36): 8687-8693.

Kim, H., A.L. Sørensen, J. Hur, L. Heimbürger, D. Hahm, T. Siek Rhee, S. Noh and S. Han. 2017. Methylmercury mass budgets and distribution characteristics in the western Pacific Ocean. *Environmental Science and Technology*, 51(3): 1186-1194.

Lamborg, C.H., C.R. Hammerschmidt and K.L. Bowman. 2016. An examination of the role of particles in oceanic mercury cycling. *Philosophical Transactions of the Royal Society A: Mathematical, Physical and Engineering Sciences*.

Lamborg, C.H., C.R. Hammerschmidt, K.L. Bowman, G.J. Swarr, K.M. Munson, D.C. Ohnemus, P.J. Lam, L. Heimbürger, M.J.A. Rijkenberg and M.A. Saito. 2014. A global ocean inventory of anthropogenic mercury based on water column measurements. *Nature*, 512: 65-68.

Lehnherr, I., V.L. Louis, H. Hintelmann and J.L. Kirk. 2011. Methylation of inorganic mercury in polar marine waters. *Nature Geoscience*, 4: 298-302.

Lomas, M.W. and Lipschultz, F. 2006. Forming the primary nitrite maximum: Nitrifiers or phytoplankton? *Limnology and Oceanography*, 51(5): 2453-2467.

Lücker, S., B. Nowka, T. Rattei, E. Spieck and H. Daims. 2013. The genome of *Nitrospina gracilis* illuminates the metabolism and evolution of the major marine nitrite oxidizer. *Frontiers in Microbiology* 4.

Mason, R.P., A.L. Choi, W.F. Fitzgerald, C.R. Hammerschmidt, C.H. Lamborg, A.L. Sørensen and E.M. Sunderland. 2012. Mercury biogeochemical cycling in the ocean and policy implications. *Environmental Research*, 119: 101-117.

Mason, R.P. and Fitzgerald, W.F. 1991. Mercury speciation in open ocean waters. *Water Air and Soil Pollution*, 56: 779-789.

Mason, R.P., W.F. Fitzgerald and F.M.M. Morel. 1994. The biogeochemical cycling of elemental mercury: Anthropogenic influences. *Geochimica et Cosmochimica Acta*, 58(15): 3191-3198.

Mcllvin, M.R. and Altabet, M.A. 2005. Chemical conversion of nitrate and nitrite to nitrous oxide for nitrogen and oxygen isotopic analysis in freshwater and seawater. *Analytical Chemistry*, 77(17): 5589-5595.

Merbt, S.N., D.A. Stahl, E.O. Casamayor, E. Martí, G. W. Nicol and J.I. Prosser. 2012. Differential photoinhibition of bacterial and archaeal ammonia oxidation. *FEMS Microbiology Letters*, 327(1): 41-46.

Mergler, D., H.A. Anderson, L. Hing Man Chan, K.R. Mahaffey, M. Murray, M. Sakamoto and A.H. Stern. 2007. Methylmercury exposure and health effects in humans: a worldwide concern. *AMBIO: A Journal of the Human Environment*, 36(1): 3-11.

Monperrus, M., E. Tessier, D. Amouroux, A. Leynaert, P. Huonnic and O.F.X. Donard. 2007. Mercury methylation, demethylation and reduction rates in coastal and marine surface waters of the Mediterranean Sea. *Marine Chemistry*, 107(1): 49-63.

Munson, K.M., D. Babi and C.H. Lamborg. 2014. Determination of monomethylmercury from seawater with ascorbic acid-assisted direct ethylation. *Limnology and Oceanography: Methods*, 12: 1-9.

Munson, K.M., C.H. Lamborg, R.M. Boiteau and M.A. Saito. 2018. Dynamic mercury methylation and demethylation in oligotrophic marine water. *Biogeosciences* 15: 6451-6460.

Newell, S.E., S.E. Fawcett and B.B. Ward. 2013. Depth distribution of ammonia oxidation rates and ammonia-oxidizer community composition in the Sargasso Sea. Limnology and Oceanography, 58(4): 1491-1500.

Outridge, P.M., R.P. Mason, F. Wang, S. Guerrero and L.E. Heimbürger-Boavida. 2018. Updated global and oceanic mercury budgets for the United Nations Global Mercury Assessment 2018. *Environmental Science and Technology*, 52(20): 11466-11477.

Ortiz, V.L., R.P. Mason and J. E. Ward. 2015. An examination of the factors influencing mercury and methylmercury particulate distributions, methylation and demethylation rates in laboratory generated marine snow. *Marine Chemistry*, 177: 753-762.

Pacyna, J.M., O. Travnikov, F. De Simone, I.M. Hedgecock, K. Sundseth, E.G. Pacyna, F. Steenhuisen, N. Pirrone, J. Munthe and K. Kindbom. 2016. Current and future levels of mercury atmospheric pollution on a global scale. *Atmospheric Chemistry and Physics*, 16: 12495-12511.

Parks, J.M., A. Johs, M. Podar, R. Bridou, R.A. Hurt, S.D. Smith, S.J. Tomanicek, Y. Qian, S.D. Brown, C.C. Brandt, A.V. Palumbo, J.C. Smith, J.D. Wall, D.A. Elias and L. Liang. 2013. The genetic basis for bacterial mercury methylation. *Science*, 339(6125): 1332-1335.

Pirrone, N., S. Cinnirella, X. Feng, R.B. Finkelman, H.R. Friedli, J. Leaner, R. Mason, A.B. Mukherjee, G.B. Stracher, D.G. Streets and K. Telmer. 2010. Global mercury emissions to the atmosphere from anthropogenic and natural sources. *Atmospheric Chemistry and Physics*, 10: 5951-5964.

Podar, M., C.C. Gilmour, C.C. Brandt, A. Soren, S.D. Brown, B.R. Crable, A.V. Palumbo, A.C. Somena-Hally and D.A. Elias. 2015. Global prevalence and distribution of genes and microorganisms involved in mercury methylation. *Science Advances*, 1(9).

Schartup, A.T., U. Ndu, P.H. Balcom, R.P. Mason and E.M. Sunderland. 2015. Contrasting effects of marine and terrestrially derived dissolved organic matter on mercury speciation and bioavailability in seawater. *Environmental Science and Technology*, 49(10): 5965-5972.

Schartup, A.T., A.L. Sørensen, H. Angot, K. Bowman and N.E. Selin. 2022. What are the likely changes in mercury concentration in the Arctic atmosphere and ocean under future emissions scenarios? *Science of The Total Environment*, 836.

Schroeder, W.H. and Munthe, J. 1998. Atmospheric mercury – An overview. *Atmospheric Environment*, 32(5): 809-822.

Shiozaki, T., M. Ijichi, K. Isobe, F. Hashihama, K. Nakamura, M. Ehama, K. Hayashizaki, K. Takahashi, K. Hamasaki and K. Furuya. 2016. Nitrification and its influence on biogeochemical cycles from the equatorial Pacific to the Arctic Ocean. *The ISME Journal*, 10: 2184-2197.

Shiozaki, T., M. Ijichi, A. Fujiwara, A. Makabe, S. Nishino, C. Yoshikawa and N. Harada. 2019. Factors regulating nitrification in the Arctic Ocean: Potential impact of sea ice reduction and ocean acidification. *Global Biogeochemical Cycles*, 33(8): 1085-1099.

Sonke, J.E., R. Teisserenc, L. Heimbürger-Boavida, M.V. Petrova, N. Marusczak, T. Le Dantec, A.V. Chupakov, C. Li, C.P. Tackray, E.M. Sunderland, N. Tananaev and O.S. Pokrovsky. *Earth, Atmospheric, and Planetary Sciences*, 115(50): E11586-E11594.

Sørensen, A.L., D.J. Jacob, A.T. Schartup, J.A. Fisher, I. Lehnherr, V.L. St. Louis, L. Heimbürger-Boavida, J.E. Sonke, D.P. Krabbenhoft and E.M. Sunderland. 2016. A mass budget for mercury and methylmercury in the Arctic Ocean. *AGU: Global Biogeochemical Cycles*.

Sunderland, E.M. 2007. Mercury exposure from domestic and imported estuarine and marine fish in the United States seafood market. *Environmental Health Perspective*, 115(2): 235-242.

Sunderland, E.M., D.P. Krabbenhoft, J.W. Moreau, S.A. Strode and W.M. Landing. 2009. Mercury sources, distribution, and bioavailability in the North Pacific Ocean: Insights from data and models. *Global Biogeochemical Cycles*, 23(2).

Stabeno, P.J., S. Bell, W. Cheng, S. Danielson, N. Kachel and C.W. Mordy. 2016. Long-term observations of Alaska Coastal Current in the northern Gulf of Alaska. *Deep Sea Research Part II: Tropical Studies in Oceanography*, 132: 24-40.

Starr, L.D., M.J. McCarthy, C.R. Hammerschmidt, A. Subramaniam, M.C. Despins, J.P. Montoya and S.E. Newell. *in review*. Mercury methylation linked to nitrification in the tropical North Atlantic Ocean. *Marine Chemistry*.

Strom, S.L., M. Brady Olson, E.L. Macri and C.W. Mordy. 2006. Cross-shelf gradients in phytoplankton community structure, nutrient utilization, and growth rate in the coastal Gulf of Alaska. *Marine Ecology Progress Series*, 328: 75-92.

Swift, J.H. and Aagaard, K. 1976. Upwelling near Samalga Pass. *Limnology and Oceanography*, 21(3):339-408.

Tada, Y., K. Marumoto and A. Takeuchi. 2020. *Nitrospina*-like bacteria are potential mercury methylators in the mesopelagic zone in the East China Sea. *Frontiers in Microbiology*.

Tada, Y., K. Marumoto and A. Takeuchi. 2021. *Nitrospina*-like bacteria are dominant potential mercury methylators in both the Oyashio and Kuroshio regions of the Western North Pacific. *Environmental Microbiology*.

United Nations. 2013. Minamata Convention on Mercury.

Villar, E., L. Cabrol and L. Heimbürger-Boavida. 2020. Widespread microbial mercury methylation genes in the global ocean. *Environmental Microbiology Reports*, 12(3): 277-287.

Wang, K., K.M. Munson, A. Beaupre-Laperriere, A. Mucci, R.W. Macdonald and F. Wang. 2018. Subsurface seawater methylmercury maximum explains biotic mercury concentrations in the Canadian Arctic. *Scientific Reports*, 8.

Ward, B.B. 2008. Nitrification in marine systems. *Nitrogen in the marine environment,* 2: 199-261.

Zhang, Y., Z. Song, S. Huang, P. Zhang, Y. Peng, P. Wu, J. Gu, S. Dutkiewicz, H. Zhang, S. Wu, F. Wang, L. Chen, S. Wang and P. Li. 2021. Global health effects of future atmospheric mercury emissions. *Nature Communications*, 12.

Zolkos, S., A.V. Zhulidov, T.Y. Gurtovaya, V.V. Gordeev, S. Berdnikov, N. Pavlova, E.A. Kalko, Y.A. Kuklina, D.A. Zhulidov, L.S. Kosmenko, A.I. Shiklomanov, A. Suslova, B.M. Geyman, C.P. Thackray, E.M. Sunderland, S.E. Tank, J.W. McClelland, R.G.M. Spencer, D.P. Krabbenhoft, R. Robarts, R.M. Holmes. 2022. Multidecadal declines in particulate mercury and sediment export from Russian rivers in the pan-Arctic basin. *Proceedings of the National Academy of Science*, 119(14).

VI. SUPPLEMENTAL MATERIAL

Table S1: *Sampling station data for each cruise (NGA LTER: SKQ2021-06S, BAITMIX: SKQ2021-07S, Mercury Cycling in the Arctic: SKQ2021-08S) across five sampled sub-Arctic regions.*

Region	Station	Sampling Date	Latitude	Longitude	Cruise	Bottom Depth (m)	Sampling Depth (m)
Gulf of Alaska	MID2	04/28/2021	60.101	-145.647	SKQ2021-06S	118	20
	GAK4	05/02/2021	59.409	-149.049	SKQ2021-06S	200	20
	KOD2	04/24/2021	58.130	-151.386	SKQ2021-06S	125	40
	KOD5	04/24/2021	57.785	-150.760	SKQ2021-06S	88	40
	KOD10	04/25/2021	57.204	-149.723	SKQ2021-06S	2518	20
Unimak Pass	UP1	05/14/2021	54.411	-164.839	SKQ2021-07S	165	40
	STN16	06/09/2021	54.463	-166.037	SKQ2021-08S	540	30
Bering Sea	STN1	05/22/2021	59.000	-172.999	SKQ2021-08S	105	20
	STN2	05/23/2021	62.005	-168.553	SKQ2021-08S	34	15
	STN14	06/06/2021	62.999	-167.366	SKQ2021-08S	37	15
	STN15	06/07/2021	60.830	-168.825	SKQ2021-08S	38	15
Bering Strait	STN3	05/24/2021	65.004	-167.685	SKQ2021-08S	33	15
	STN13	06/05/2021	65.519	-168.371	SKQ2021-08S	54	15
Chukchi Sea	STN4	05/25/2021	68.999	-167.342	SKQ2021-08S	51	18
	STN5	05/27/2021	70.017	-166.122	SKQ2021-08S	48	20
	STN6	05/29/2021	70.391	-164.198	SKQ2021-08S	44	12
	STN7	05/30/2021	70.137	-165.056	SKQ2021-08S	42	14
	STN9	06/01/2021	69.760	-166.933	SKQ2021-08S	46	15

Table S2: *Ambient mercury, rate measurements, and Nitrospina-specific hgcA-like gene abundance across all stations.*

Region	Station	Sampling Depth (m)	MeHg (fM)	HgT (pM)	MeHg:HgT (%)	Hg Methylation (10^{-3} d^{-1})	Nitrification (nM d^{-1})	Gene Abundance (copies mL^{-1})
Gulf of Alaska	MID2	20	N.D.	N.D.	N.D.	2.3	3.48	6041
	GAK4	20	N.D.	N.D.	N.D.	7.8	0.17	1979
	KOD2	40	N.D.	2.03	N.D.	3.5	1.34	379
	KOD5	40	N.D.	1.84	N.D.	4.8	1.31	398
	KOD10	20	21.43	1.63	1.41	2.5	0.07	1318
Unimak Pass	UP1	40	N.D.	N.D.	N.D.	5.8	N.D.	N.D.
	STN16	30	N.D.	N.D.	N.D.	1.1	N.D.	236
Bering Sea	STN1	20	1.42	0.17	0.90	4.4	2.93	6278
	STN2	15	8.14	0.96	0.91	2.0	0.54	439
	STN14	15	23.05	0.81	3.05	7.9	N.D.	361
	STN15	15	3.10	1.73	0.19	3.1	N.D.	503
Bering Strait	STN3	15	N.D.	1.58	N.D.	2.7	0.86	2635
	STN13	15	37.09	0.61	6.50	8.0	0.17	3192
Chukchi Sea	STN4	18	4.35	0.34	1.37	4.0	1.20	97
	STN5	20	16.66	0.97	1.84	1.1	4.54	297
	STN6	12	34.52	0.70	5.31	8.2	2.53	4378
	STN7	14	9.36	0.64	1.56	2.0	0.18	2243
	STN9	15	39.43	1.11	3.83	3.4	0.79	2378